INTERNATIONAL JOURNAL OF
NUMERICAL ANALYSIS AND MODELING
Volume 12, Number 4, Pages 684–703

© 2015 Institute for Scientific
Computing and Information

NUMERICAL INVERSION SCHEMES FOR MAGNETIZATION USING AEROMAGNETIC DATA

YILE ZHANG, YAU SHU WONG, JIAN DENG, SHA LEI, AND JULIEN LAMBERT

Abstract. The re-weighted regularized conjugate gradient (RRCG) method has been a popular algorithm for magnetic inversion problems. In this work, we show that for a two-dimensional problem with uniform field data, the resulting coefficient matrix to be inverted has a symmetric Block-Toeplitz Toeplitz-Block (BTTB) structure. Taking advantage of the BTTB properties, the storage and computational complexity can be significantly reduced, so that the efficiency of the RRCG method is greatly improved and it is now capable of dealing with much larger system with a modest computing resource. This paper also investigates various numerical inversion schemes including the CG type and multigrid (MG) methods. It has been demonstrated that the MG is an efficient and robust numerical tool for magnetic field inversion. Not only the MG produces a rapid convergence rate, the performance is not sensitive when applying to noisy data. Numerical simulations using synthetic data and real field data are reported to confirm the effectiveness of the MG method.

Key words. Magnetic inversion, Numerical algorithm, Toeplitz matrix, Multigrid method, Conjugate gradient method.

1. Introduction

Magnetic field survey is one of the most popular geophysical techniques for fast mapping of large areas in geophysical and environmental study. The survey consists of mapping one or more components of the earth geomagnetic field in order to analyze the magnetic anomalies. The magnetic anomalies mapping can be generally used as a tool to many geological applications such as estimating the basement topography, assessing the depth in oil exploration and the magnetic polarization in mineral prospecting.

Inversion model is closely related to the forward computation, and this is a key step in the geophysical survey. For the magnetic field inversion problem, the model can be expressed mathematically as an integral formulation. The inversion solution can be obtained by solving a resulting system of linear equations $Au = b$, where b is the observation magnetic field data. The major challenge of the inversion problem is due to the fact that the matrix A is often large, dense and ill-conditioned [13], thus inverting the system by a direct method is not practical and employing an numerical iterative scheme will require enormous computing resource.

Although some works have been reported for a 3-D magnetic field inversion [18, 20], in many cases, 2-D model is more preferred, this is particularly true for the aero-magnetic survey. The simplicity of the 2-D model also make the 2-D inversion practical and efficient. The inversion for tabular magnetic anomalies or thin layer magnetic anomalies have been investigated in [15, 21, 2, 22, 26].

For the irregular raw data, it can be rewritten into a uniform data conveniently by the use of a regridding procedure. Many efficient methods have been developed, for instance, Briggs [4] proposed a minimum curvature method to regrid non-uniform

Received by the editors October 14, 2014.
2000 *Mathematics Subject Classification.* 86A20, 86A22, 86A30.
This research was supported by the Natural Sciences and Engineering Research Council of Canada and MITACS Accelerate Program.

data. Cordell and Blakely [12, 3] presented an equivalent layer method (ELM), in which a fictitious source layer is introduced and the non-uniform data points are interpolated on the uniform grid. The advantage of implementing the ELM has been reported by Cooper [11], and a comparative study of ELM and the minimum curvature method can be found in [19].

The most important feature for considering a uniform field data is that the resulting coefficient matrix for the inversion problem is a symmetric Block-Toeplitz Toeplitz-Block (BTTB) matrix. Consequently, efficient and accurate numerical inversion algorithms can be developed, and the matrix-vector product can be implemented efficiently using a Fast Fourier Transform (FFT). In some other work, the BTTB structure has already been noticed. Rauth and Strohmer [23] investigated the potential field gridding problem by interpolating the non-uniform field data into a uniform field data, where the trigonometric polynomial is used to approximate the magnetic field, and the coefficients of the polynomial are computed by solving a BTTB system. However, in our work, the BTTB structure is derived directly from magnetic forward formulation. To the best of our knowledge, no systematic investigation on the BTTB structure and construction of numerical schemes utilizing the special BTTB properties in magnetic inversion problem has been carried out.

In this paper, we investigate numerical schemes for magnetic data inversion. Particular attention is focused on incorporating the BTTB structure to develop efficient numerical inversion algorithms based on the conjugate gradient (CG) type methods and the multigrid (MG) technique. The CG type methods include the standard CG (CG), preconditioned CG (PCG) and the re-weighted regularized CG (RRCG) method. A comparative study of the MG and CG type methods is presented, and the performance of these methods is validated by numerical simulations applied to the synthetic field data and the real geophysical data.

2. Forward Model

Assuming that the magnetic data covers an area which is filled with a set of vertical prisms with arbitrary horizontal section and the bottom at infinity, the magnetic anomaly reduced to the pole is given by a layer of poles on the top of each prism as shown in Figure 1.

The magnetization is defined as the magnetic moment ($\mathbf{M}$) per volume as

$$\boldsymbol{J} = \frac{d\mathbf{M}}{dv}, \tag{1}$$

which is induced by the earth magnetic field, and is the source of the magnetic anomaly. To determine the magnetic field generated by the magnetization, the concept of magnetic scalar potential ψ is introduced. When there is no free current, the magnetic scalar potential can be used to determine the magnetic H-field especially for the permanent magnets in the following way,

$$\mathbf{H} = -\nabla\psi. \tag{2}$$

It is known that the magnetic potential generated by $d\mathbf{M}$ at an arbitrary point P is defined by $d\psi = \frac{d\mathbf{M}\cdot\mathbf{r}}{\rho}$, where $\mathbf{r}$ is a coordinate of P, and ρ is the distance from P to dv. According to (1),

$$d\psi = -\left[\mathbf{J}\cdot\nabla(\frac{1}{\rho})\right] dv. \tag{3}$$

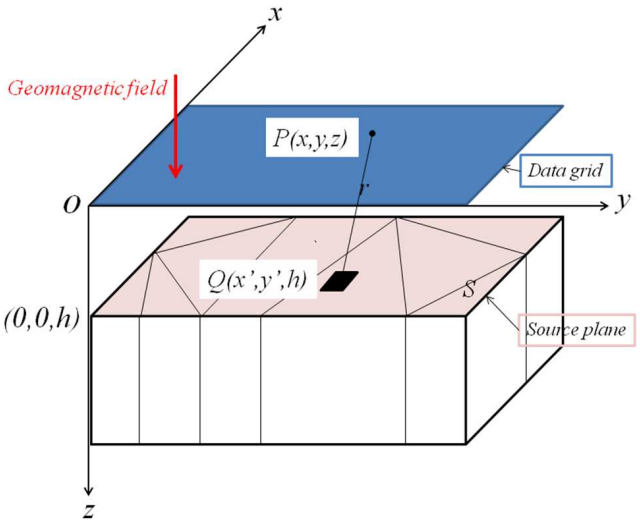

FIGURE 1. Forward Model.

Thus, the magnetic potential at the point P generated by a prism is given by

$$\psi = -\int_V \left[\mathbf{J}\cdot\nabla(\frac{1}{\rho})\right] dv. \tag{4}$$

According to the Gauss formula, (4) can be further rewritten as

$$\psi = \int_S \frac{(\mathbf{J}\cdot dS)}{\rho} - \int_V (\frac{\mathrm{div}\mathbf{J}}{\rho}) dv. \tag{5}$$

By assuming that in each prism, the value of magnetization $\mathbf{J}$ is uniform, and the magnetization in the prisms have the same direction, then $\mathrm{div}\mathbf{J} = 0$, and only the first term in (5) is retained. The integral on the side facing the prisms can be neglected, since the bottom is assumed to be infinitely deep and the upper surface can be regarded as the source plane. Hence, (5) can be simplified as

$$\psi = \int_S \frac{J_n}{\rho} dS, \tag{6}$$

where J_n is the vertical magnetization in nth prism. Here, the magnetic potential ψ is a function of the coordinate of point P. If we denote the position of dv as Q, and the coordinate of Q as $\mathbf{r}'$, then $\rho = |\mathbf{r} - \mathbf{r}'|$. According to (2), the magnetic field generated by each prism is given by

$$\mathbf{H} = -\nabla\psi = -\nabla \int_S \frac{J_n}{|\mathbf{r} - \mathbf{r}'|} dS, \tag{7}$$

in which the vertical magnetic field is

$$H_z = \int_S \frac{J_n(z - z')}{|\mathbf{r} - \mathbf{r}'|^3} dS. \tag{8}$$

Now, considering all prisms as a whole, thus the magnetic field at the point P is generated by all prisms. By (8), denote the J_n as a function of coordinate, then the magnetic anomaly is described by the convolution of two functions: one depending on the positions of the observations and the other describing the distribution of

magnetization as the following:

$$H_z(x,y,z) = \iint_S m(x',y',z')G(x,y,z,x',y',z')dx'dy', \tag{9}$$

where

$$G(x,y,z,x',y',z') = \frac{z-z'}{[(x-x')^2+(y-y')^2+(z-z')^2]^{\frac{3}{2}}}. \tag{10}$$

3. BTTB Structure

Using the standard discretization procedure, the forward model (9) can be discretized as

(11)

$$d(x(i),y(i),z) = \sum_{j=1}^{N}\sum_{k=1}^{M} G(x(i),y(i),z,x'(j),y'(k),h)m(x'(j),y'(k),h)\triangle x\triangle y,$$

where z is the vertical coordinate of the observation point, and h is the depth of the magnetization. Now (11) can be further rewritten as

$$d(x(i),y(i),z) = \sum_{l=1}^{N\times M} G(x(i),y(i),z,x'(l),y'(l),h)m(x'(l),y'(l),h)\triangle x\triangle y, \tag{12}$$

where

$$G(i,l,h) = \frac{h-z}{[(x(i)-x(l))^2+(y(i)-y(l))^2+(h-z)^2]^{\frac{3}{2}}}.$$

Therefore, equation (9) can be approximated by the linear system

$$d = Am, \tag{13}$$

where d is the $(N\times M)$-by-1 observation data representing the anomalous magnetic field, m is $(N\times M)$-by-1 column vector corresponding to the magnetization, and A is a full and symmetric $(N\times M)$-by-$(N\times M)$ matrix. Consider the case where the observation field data is 512-by-512, then the resulting coefficient matrix A is 262144-by-262144. Therefore, the storage requirement for A is of the order $(N\times M)^2 \sim 6.8*10^{10}$. Solving the linear system by a direct method is impossible or very impractical since the work will be of order $(N\times M)^3 \sim 1.8*10^{16}$. However, seeking a numerical solution by an iterative scheme would also require enormous computing resources since the computational work is typically dependent on the matrix-by-vector operations which is $\mathrm{O}((N\times M)^2) \sim 6.8*10^{10}$.

One of the major contributions of the present work is to recognize that the resulting matrix A is a symmetric Block-Toeplitz Toeplitz-Block system, and this will lead to a tremendous saving in the storage for the coefficient matrix and offer many efficient algorithms for solving the BTTB system. The BTTB matrix generated in our problem is given as the following:

$$T_{mn} = \begin{bmatrix} T_{(0)} & T_{(1)} & \cdots & T_{(m-2)} & T_{(m-1)} \\ T_{(1)} & T_{(0)} & T_{(1)} & \cdots & T_{(m-2)} \\ \vdots & T_{(1)} & T_{(0)} & \ddots & \vdots \\ T_{(m-2)} & \cdots & \ddots & \ddots & T_{(1)} \\ T_{(m-1)} & T_{(m-2)} & \cdots & T_{(1)} & T_{(0)} \end{bmatrix}, \tag{14}$$

where the blocks $T_{(i)}$, for $i \leq m-1$, are themselves symmetric Toeplitz matrices of order n and each defined by the following,

$$T_n = \begin{bmatrix} t_0 & t_1 & \cdots & t_{n-2} & t_{n-1} \\ t_1 & t_0 & t_1 & \cdots & t_{n-2} \\ \vdots & t_1 & t_0 & \ddots & \vdots \\ t_{n-2} & \cdots & \ddots & \ddots & t_1 \\ t_{n-1} & t_{n-2} & \cdots & t_1 & t_0 \end{bmatrix}. \tag{15}$$

It is important to note that the first row or first column contains all the information of the matrix, therefore, the entire BTTB matrix can be compactly stored by a $(N \times M)$-by-1 vector. For the same problem with given 512-by-512 observation field data, the storage is now $O(2.6 * 10^5)$ instead of $O(6.8 * 10^{10})$ using a direct storage.

Even though the BTTB matrix (14) is a dense matrix, computation for the matrix-vector product can be efficiently implemented. It has already been reported in [14] that a circulant matrix C_n can be diagonalized by the Fourier matrix F_n, i.e.,

$$C_n = F_n^* \Lambda_n F_n,$$

where Λ_n is a diagonal matrix containing the eigenvalues of C_n. Therefore, the matrix-vector product $C_n y$ and $C_n^{-1} y$ can be computed by fast Fourier transform, which can also be implemented by a highly parallel algorithm. Similarly, the product of a Block-Circulant Circulant-Block (BCCB) matrix and vector can be computed by a two-dimensional FFT. Considering the fact that the $(N \times M)$-by-$(N \times M)$ BTTB matrix can be embedded into $(2N \times M)$-by-$(2N \times M)$ BCCB matrix [7], then the matrix-vector product $T_{mn} v$ can also be computed by FFT. The computational cost is now reduced to $O((N \times M) \log(N \times M))$, which is much smaller than the original cost $O((N \times M)^2)$. For the example of the observation field data given by 512-by-512, the work per iteration by using a CG method is now $O(1.4 * 10^6)$ instead of $O(6.8 * 10^{10})$ without taking advantage of the BTTB properties.

By recognizing the matrix A has the symmetric BTTB structure, the dense matrix can now be stored efficiently in a compact form, and the matrix-vector product can be computed effectively by a fast Fourier transform.

4. Numerical Inversion Schemes

In this section, we present iterative numerical schemes for solving the magnetic inversion problem given by Equation (13). The iterative schemes are based on the Conjugae Gradient (CG) type methods including standard CG, preconditioned CG (PCG), re-weighted regularized CG (RRCG) and the multigrid (MG) technique.

4.1. Conjugate gradient type methods. The conjugate gradient (CG) method is one of the most powerful iterative schemes for solving large positive definite system, and it has been widely used in solving the BTTB system [9].

However, a drawback of the CG method relates to the robustness, namely the performance is sensitive to the perturbation or noise in the observation field data. To enhance the reliability, a general approach based on the Tikhonov regularization method [27] is usually incorporated with the CG method. The regularized CG schemes are frequently employed in geophysical applications. Recall that the inversion is achieved by solving the linear equation (13), where A is the symmetric BTTB matrix, d is the observation magnetic field data and m is the magnetization

to be inverted. Now consider the corresponding parametric functional given by the following form:

$$P^{\alpha}(m,d) = ||W_d A m - W_d d||^2 + \alpha ||W_m m - W_m m_{apr}||^2, \tag{16}$$

where W_d and W_m are weighting matrices for the data and model, respectively. In most applications, W_d is a diagonal matrix, m_{apr} is a vector which contains priori geologic information and $||\cdot||$ denotes the Euclidean norm in the spaces of data and models [27]. The regularized problem is an approximation to the original equation, but it will be more well-posed than the original problem. Since the regularization deviates from the original problem, to reduce the deviation, a re-weighted regularization strategy is introduced. Let the regularization parameter α be self-adaptive, the re-weighted regularized conjugate gradient (RRCG) method is given as the following [27]:

(1) $r_n = Am_n - d$, $s_n = W_{en}W_m(m_n - m_{apr})$,
(2) $I_n^{\alpha_n} = I^{\alpha_n}(m_n) = A^T W_d^2 r_n + \alpha_n W_{en} W_m s_n$,
(3) $\beta_n^{\alpha_n} = ||I_n^{\alpha_n}||^2 / ||I_{n-1}^{\alpha_{n-1}}||^2$,
(4) $\tilde{I}_n^{\alpha_n} = I_n^{\alpha_n} \tilde{I}_{n-1}^{\alpha_{n-1}}$, $\tilde{I}_0^{\alpha_0} = I_0^{\alpha_0}$,
(5) $\tilde{k}_n^{\alpha_n} = (\tilde{I}_n^{\alpha_n T} I_n^{\alpha_n}) / \left[\tilde{I}_n^{\alpha_n T}(A^T W_d^2 A + \alpha W_{en}^2 W_m^2)\tilde{I}_n^{\alpha_n}\right]$,
(6) $m_{n+1} = m_n - \tilde{k}_n^{\alpha_n} \tilde{I}_n^{\alpha_n}$, $\gamma = ||s_{n+1}||^2 / ||s_n||^2$,
(7) $\alpha_{n+1} = \alpha_n$, if $\gamma \le 1$, and $\alpha_{n+1} = \alpha_n / \gamma$, if $\gamma > 1$,

where the W_{en} is the error estimation matrix. The initial regularization parameter α_0 is chosen according to the L-curve strategy [16]. Moreover, $W_d = I$, $W_{en} = I$, $m_{apr} = 0$, $W_m = I$ are chosen in the following computation.

In addition to the RRCG method, the preconditioned CG (PCG) methods are also popular in solving the BTTB system [10]. Various preconditioners have been designed for the BTTB system [24, 17, 6], and the PCG algorithm is given as the following [1]:

(1) $r_0 = b - Am_0$,
(2) $p_0 = r_0$,
(3) $\alpha_{n-1} = \frac{r_{n-1}^T p_{n-1}}{P_{n-1}^T A P_{n-1}}$,
(4) $m_n = m_{n-1} + \alpha_{n-1} p_{n-1}$,
(5) $r_n = r_{n-1} - \alpha_{n-1} A p_{n-1}$,
(6) Solve $B^T B z_n = r_n$ for z_n,
(7) $p_n = z_n - \frac{z_n^T A p_{n-1}}{p_{n-1}^T A p_{n-1}} p_{n-1}$,

where $B^T B$ is known as a preconditioner. By choosing $B = I$, it reverts to the standard CG. In the present work, the preconditioner $B^T B$ is chosen as

$$B^T B = (C_r)^{\frac{1}{4}} = F_{mn}^* \Lambda^{\frac{1}{4}} F_{mn}$$

where C_r is the BCCB matrix given by Chan's preconditioner [7], F_{mn} is the corresponding Fourier matrix, and Λ is the eigenvalue of matrix C_r. The regularized PCG [8] has also been applied to other BTTB system related to image processing problems.

4.2. Multigrid techniques. It is well-known that the convergence of the CG type methods depends on the condition number of the matrix A. In magnetic inversion problems, the matrix is usually very ill-conditioned and with a large condition number. Multigrid (MG) technique is developed based on multilevel iterative methods, and it has generally been regarded that MG is an optimal iterative method for

solving large positive definite systems from elliptic partial differential equations. The technique is optimal since the convergence rate is apparently optimal and independent of the condition number of A and the size of the linear system.

When solving a linear system by a classical relaxation scheme based on the Jacobi or Gauss-Seidel method, we note that the high frequency error can be eliminated very quickly, but it is hard to remove the low frequency error. Consequently, a rapid error reduction is typically observed at the initial stage, and after that the error decreases very slowly leading to a slow convergence rate.

Suppose we want to solve a linear system given by $Au = b$, instead of applying an iterative scheme directly to the system, we now consider the solution being computed by applying a relaxation scheme to multilevel or multigrid systems

$$A^j u^j = b^j,$$

where A^j denotes the matrix at different grid levels with $A^1{=}A$ known as the finest grid, and the matrices A^j, $j = 2, 3, \cdots$ are referred as the coarse grid levels. The coefficient matrix A^j for $j > 1$ can be constructed using the same way as for A^1 but with a coarser mesh. The superior performance of a MG method is achieved due to the fact that the low frequency error on the fine grid can be regarded as the high frequency error on the coarse gird. Thus by employing a relaxation scheme to a sequence of various grid levels, the high and low frequency error components can be eliminated rapidly and this ensures a fast convergence rate for a MG method.

The idea of a MG approach can be easily explained by a two-grid method as illustrated in Figure 2.

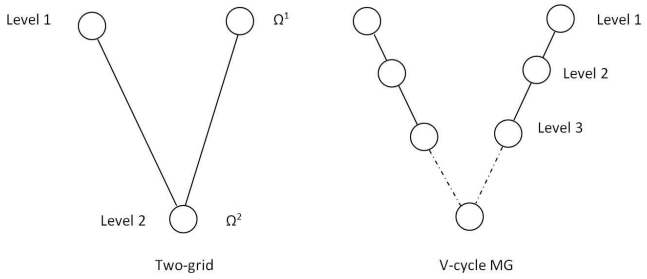

FIGURE 2. Two-grid and V-cyle MG.

Recall that if $\bar{u}$ is the computed solution of $Au = b$, the residual is defined by

$$r = b - A\bar{u} = A(u - \bar{u}) = Ae, \tag{17}$$

where e is the error vector. By solving $Ae = r$, we can then improve the numerical solution, such that

$$u = \bar{u} + e. \tag{18}$$

Let Ω^1 and Ω^2 denote the fine grid (i.e. level 1) and the coarse grid (i.e. level 2). In a two-grid method, starting with an initial approximation u^0, the algorithm is given as

(1) In Ω^1, apply relaxation ν_1 time, $u^1 \to S(u^1, b^1)$,
(2) Compute residual and transfer from Ω^1 to Ω^2:

$$r^1 = b^1 - A^1 u^1,\ r^2 = R_1^2 r^1,$$

(3) In Ω^2, solve the error equation: $A^2 e^2 = r^2$,

(4) Interpolate error from Ω^2 to Ω^1 and improve the approximation: $u^1 \rightarrow u^1 + I_2^1 e^2$,
(5) Repeat the procedure until a stopping criteria such as $||r^1|| < \varepsilon$ is achieved.

Here, $S(u^1, b^1)$ denotes a smoothing or a relaxation process which will be defined shortly. Dropping the superscript index for the matrix A, let $A = D - L - L^T$, u^0 is an initial approximation, the weighted Jacobi relaxation is selected as a smoothing operator such that $S(u^1, b^1)$ is defined by

$$u^1 = [(1-\omega)I + \omega D^{-1}(L + L^T)]u^0 + \omega D^{-1} b^1,$$

where ω is a parameter, which can be estimated by a formula proposed in [25]:

$$\omega \leq \frac{a_{0,0}}{\rho(A)}, \tag{19}$$

where $a_{0,0}$ is the first element of the matrix A and $\rho(A)$ is the spectral radius of A. Note that R_1^2 is a restriction operator which is used to transfer the residual from a fine grid to coarse grid and I_2^1 is an interpolation operator which is used to interpolate the error from a coarse grid to a fine grid. Also, (1) is generally referred as the smoothing step, and (3) is the correction step in an MG cycle.

It should be recognized that solving the error equation in step 3 is a system of the same type as the original system. Therefore, by repeatedly applying a two-grid method, we can construct a multigrid method, and the V-cycle MG is shown in Figure 2. The details on the construction of the coarse grid coefficient matrices, the restriction and interpolation operators can be found in [5].

5. Numerical Simulations

To validate the effectiveness of various iterative schemes presented in the previous section, we consider the following test cases. The CG type methods and the MG will be assessed based on their efficiency, accuracy and robustness. The computation are carried out using a laptop computer with Intel i7-3632QM 2.2 Hz and 12G RAM. For the MG method, the computation is based on a V-cycle using three grid levels with one relaxation at each grid during the smoothing and correction steps.

5.1. Synthetic data. The first test case is constructed based on a synthetic data set. Figure 3 illustrates the initial magnetization distribution, and it is considered to be the exact solution for the magnetic inversion problem. In Figure 4, we display the computed solutions of the magnetic field data generated by the synthetic magnetization at different depth h = 50m, 100m, 200m, 250m, respectively. To evaluate the performance of various numerical inversion schemes, let the relative error (RE) be defined as:

$$RE = \frac{||U_{inv} - U_{exact}||_\infty}{||U_{exact}||_\infty} \times 100\%, \tag{20}$$

where U_{inv} is the computed inverse solution, U_{exact} is the exact solution.

In Table 1, we list the condition number of the coefficient matrix for a range of depths from h = 50m to 250m. The condition number increases as the depth is increasing. Since the largest condition number appears at the maximum depth, the synthetic field data at h = 250m is chosen as the test case in which the simulation data will be inverted. The stopping criterion used for the numerical inversion methods is:

$$\frac{||r_n||_\infty}{||r_0||_\infty} < tol,$$

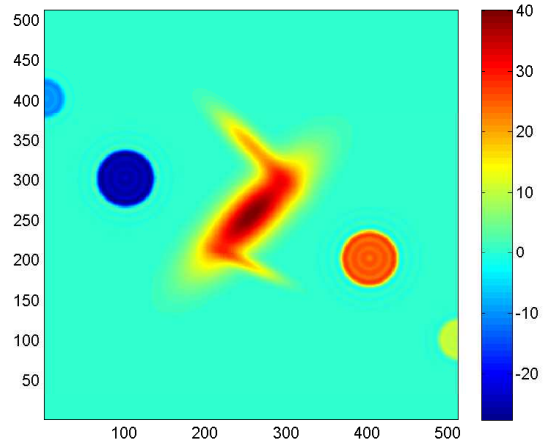

FIGURE 3. Initial magnetization distribution.

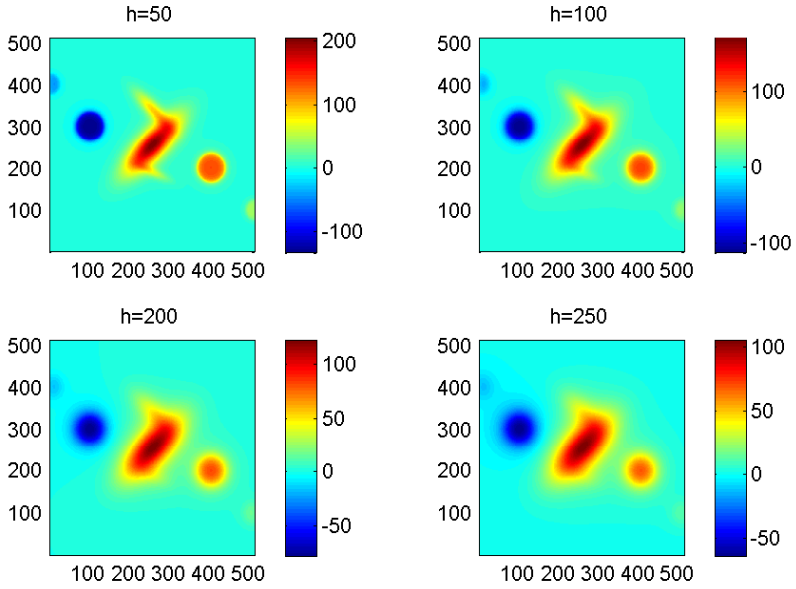

FIGURE 4. Magnetic field data at different depths.

TABLE 1. Condition number of the coefficient matrix corresponding to different depths.

Depth (m)	Condition Number
50	$1.2410*10^8$
100	$5.8372*10^8$
200	$2.1781*10^9$
250	$3.2852*10^9$

where *tol* is the tolerance of the iteration, r_n is the residue at the n-step iterations, r_0 is the initial residue. For the multigrid method, the V-cycle iteration scheme is used.

TABLE 2. Computing time and number of V-cycles of MG with various grid levels.

	Tol=10^{-3}		Tol=10^{-4}	
Level	T_{MG} (s)	N	T_{MG} (s)	N
2	7.122357	24	62.540190	203
3	3.575487	11	32.270307	97
4	3.248739	10	33.257580	103
5	3.209048	10	33.601279	103

In Table 2, we present the MG results where the level denotes the number of grid levels used in a V-cycle, T is the computing time in second, N is the number of cycles to reach a given tolerance. It is clear that good performances are achieved when the grid level is greater than two. However, for the inversion problem considered here, taking three grid levels in a V-cycle seems to suffice, and a 50% reduction in computing time over a two-grid method is achieved.

To compare the effectiveness of various numerical inversion schemes, Table 3 reports the inversion of the synthetic magnetic field data at $h = 250$m by CG, PCG, RRCG and MG methods. Here N denotes the number of iterations in CG type methods and number of cycles in MG method, and N/A means that the scheme fails to converge within 2000 iterations. In Figure 5, we plot the convergence rate for the CG, PCG, RRCG and MG method.

TABLE 3. Computing time and number of iteration of various numerical inversion for synthetic data at h=250m.

Tolerance	T_{CG} (s)	N	T_{RRCG} (s)	N	T_{PCG} (s)	N	T_{MG} (s)	N
10^{-2}	0.678969	9	9.323636	50	0.547881	7	0.585323	2
10^{-3}	1.330730	19	31.220969	167	1.175903	14	3.219449	11
10^{-4}	3.477457	53	N/A	N/A	2.692719	35	27.853854	97
10^{-5}	11.896358	182	N/A	N/A	7.668079	99	306.236100	1026

From the results presented in Table 3 and Figure 5, we note that the PCG is the most efficient in term of computing time needed to reach a given accuracy, and it then follows by the CG, MG and RRCG. Although the RRCG method has been a popular inversion algorithm used in many geophysical applications, it has a slow convergence and fails to reach a given tolerance within 2000 iterations when a small tolerance is required as indicated in Table 3. When the tolerance is in the level of 10^{-2} or 10^{-3}, the performance of the CG, PCG and MG are comparable in terms of convergence rate and the computing time required. In Figure 6, the computed solutions of the four methods for the inversion problem are displayed.

It is worthwhile to point out that the accuracy of the inversion problem cannot be guaranteed even when a small tolerance is achieved by a numerical inversion scheme. In Table 4, we present the relative errors computed by the CG and MG methods for the test cases using the synthetic data. For a given depth, the relative error can be reduced by setting a smaller tolerance. It is observed that for a fixed tolerance, the error increase, as the depth is increasing.

TABLE 4. Relative error of CG and MG method at different depths and tolerance.

	CG				MG			
Depth/Tol	10^{-2}	10^{-3}	10^{-4}	10^{-5}	10^{-2}	10^{-3}	10^{-4}	10^{-5}
50	6.55%	2.83%	1.30%	0.52%	6.72%	4.32%	2.13%	1.75%
100	11.54%	3.55%	2.33%	0.97%	14.00%	9.77%	5.09%	3.70%
200	21.78%	14.95%	8.62%	6.7%	24.11%	16.47%	10.43%	7.75%
250	24.42%	19.28%	12.97%	6.67%	27.20%	21.25%	15.00%	9.87%

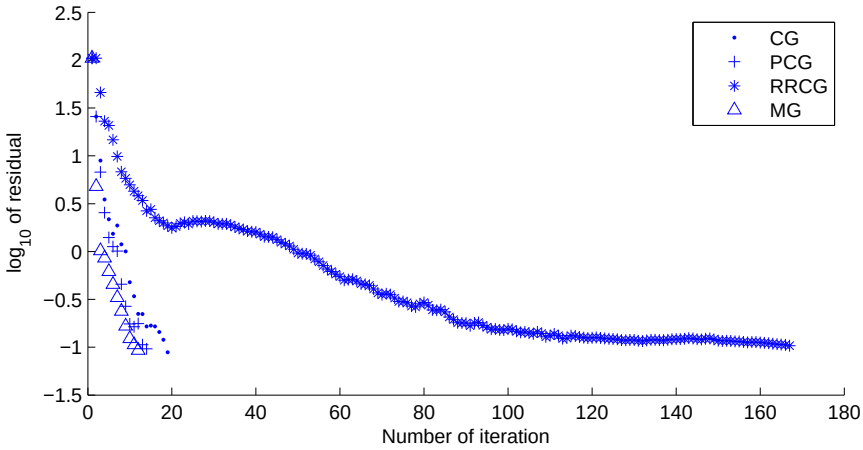

FIGURE 5. Convergence rate of CG, RRCG, PCG and MG method at tolerance=10^{-3}.

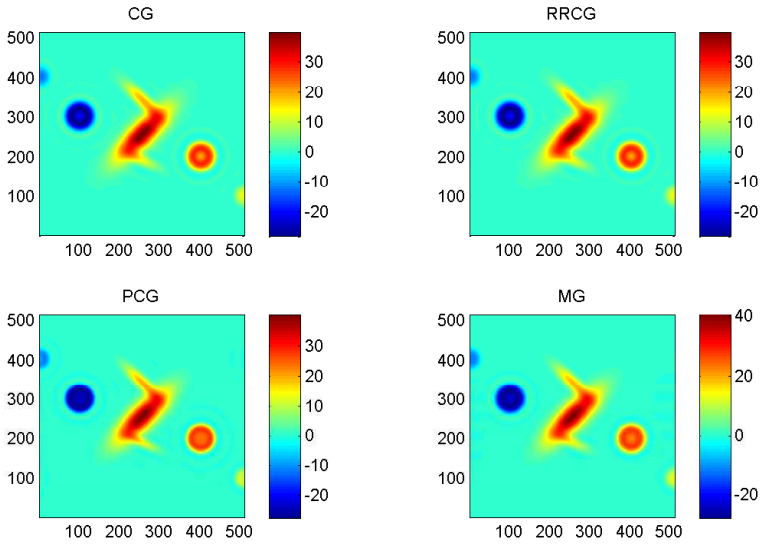

FIGURE 6. Inversion of the magnetic field at h=250m by CG, RRCG, PCG and MG method.

The test cases investigated here are constructed based on synthetic data, and they are essentially noise-free data. It should be noted that the performance of an accuracy and effective inversion algorithm may not be guaranteed if the data is contaminated with noise. In reality, the magnetic field data obtained by measurement are usually contaminated with noise. Thus, it is important to study the robustness of the inversion schemes.

To simulate test cases with noisy data, we introduce certain level of noise into the synthetic field data. Let A be the matrix resulted from the synthetic data, and E be the matrix with coefficients generated by pseudo random values in the range [0, 1] drawn from the standard normal distribution. Considering the fact that the noise in geophysical survey is produced by the measuring apparatus, then the noisy observation matrix with $\alpha\%$ noise is defined by $A' = A + \alpha\% * E$.

In Table 5 and Figure 7, the performance of the CG, PCG, RRCG and MG methods are compared when certain noise level is introduced to the synthetic data. When the noise level is 0%, the test cases revert to the original clean magnetic data with no noise. It is observed that although the CG and PCG are very effective when applied to clean data, their performances deteriorated rapidly when noise is present in the field data. The RRCG is a very reliable method, and the relative error remains almost at the same level even when a 20% noise is introduced. The MG method is not sensitive when the noise level is less than 10%, but the effect due to noise becoming noticeable when the noise level is greater than 10%. Unlike the RRCG, a regularization procedure is not incorporated to the MG method. Therefore, the performance could be improved if a suitable regularization is introduced.

TABLE 5. Relative error of CG, RRCG, PG and MG with different noise levels (%).

	0%	1%	4%	8%	12%	16%	20%
CG	24.42%	24.46%	24.25%	26.13%	$4.8*10^4$	$6.7*10^4$	$8.0*10^4$
RRCG	26.51%	26.51%	26.40%	25.63%	25.34%	25.00%	24.09%
PCG	25.80%	60.36%	$7.2*10^6$	$1.4*10^7$			
MG	27.20%	27.19%	27.24%	26.60%	27.78%	29.49%	32.90%

5.2. Real Data. From the computational results presented for the synthetic data, it is clear that both the CG and PCG methods are sensitive to the noisy data, thus the methods will not be considered for the real data inversion. In this section, only the RRCG and MG methods are employed as the numerical inversion tool for applications to real data. The real magnetic field data being tested are provided by the TerraNotes Ltd Geophysics.

Given a real geophysical data, the numerical inversion program provides an estimate of magnetization of underground rocks at certain depth h. Generally speaking, h is an unknown, and by producing a sequence of magnetization at various depths, it would provide useful information for the geologists or geophysicists to interpret the computation results and to study how dependent the results are on the variations of h.

In order to reduce the effects due to the numerical artifact which is usually introduced near the boundary, we adjust the results presented in the window in Figure 8 which is obtained by removing the shadow layer from the original data. Note that the shadow layer is very thin and consists of only five grid points, and

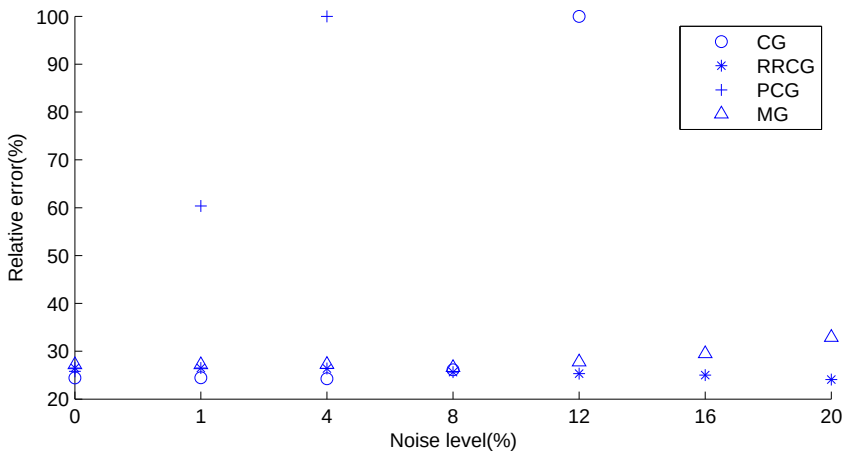

FIGURE 7. Error vs noise level for the CG, RRCG, PCG and MG method under tolerance=10^{-2}.

the original data field usually covers several hundred grid points in both directions.

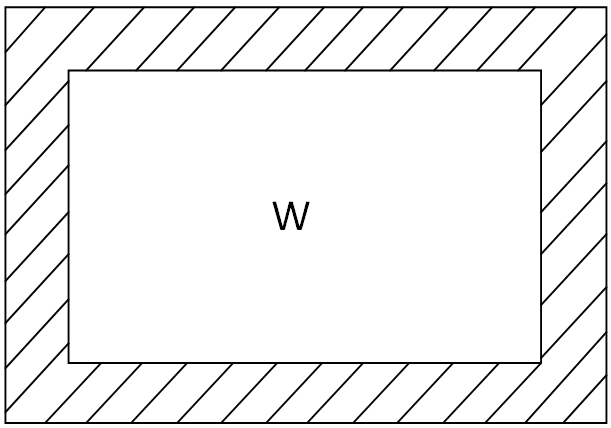

FIGURE 8. Original field data and selected window W.

5.2.1. Test case I. For the first test case, the magnetic field data covers a square area with 6000m in both the x- and y- directions, and the interval between each grids is 12m. Thus the resulting matrix is 500 by 500 as shown in the Figure 9.

Let the tolerance of the inversion program be $3 * 10^{-1}$, the computed inversion results at depth $h = 50$m, 100m and 150m using the RRCG and MG methods are shown in Figure 10. The corresponding computing time are listed in Table 6.

From the results presented in Figure 10 and Table 6, we observe that the magnetic inversions using the RRCG are in good agreement with those computed by MG. At $h = 50$m, the two results are almost identical. However, as h increases, the RRCG produces noticeable artifacts near the boundary. To investigate the sensitivity of the computed solutions, we carry out simulation with a fixed depth,

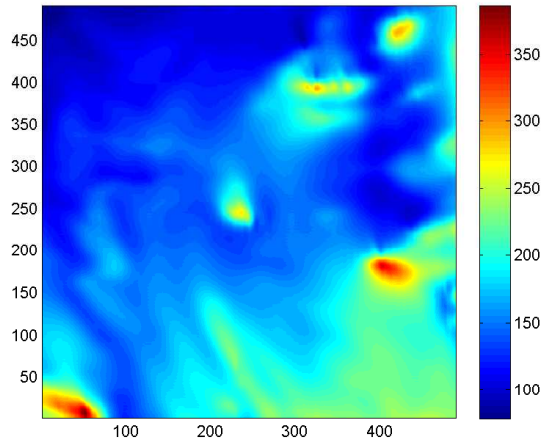

FIGURE 9. Test case I.

TABLE 6. Computing time for test case I with tolerance $3 * 10^{-1}$.

Depth (m)	T_{RRCG} (s)	T_{MG} (s)
50	1.102995	0.466652
100	2.121059	0.964995
150	3.515279	1.404609

namely h=50m and h=100m, and examine the computed solutions at two values of tolerances. Figure 11 and 12 present the numerical inversion results, and the corresponding computing time are reported in Table 7. As expected, the computed solutions are less sensitive when h is small as shown in Figure 11. Figure 12 displays the RRCG and MG results when $h = 100$m and the tolerances are set at $4 * 10^{-1}$ and $2 * 10^{-1}$, respectively. Here, the difference between the results corresponding with two tolerances are obvious. Moreover, the artifacts resulting from RRCG at $\varepsilon = 2 * 10^{-1}$ is also noticeable. From the computing time reported in Tables 6 and 7, it is clear that MG is more efficient and requires less computing time than the RRCG for all cases tested.

TABLE 7. Computing time for test case I using RRCG and MG.

Depth (m)	Tolerance	T_{RRCG} (s)	T_{MG} (s)
50	$\varepsilon = 4 * 10^{-1}$	0.894744	0.304539
50	$\varepsilon = 2 * 10^{-1}$	2.557688	0.964625
100	$\varepsilon = 4 * 10^{-1}$	1.576802	0.549794
100	$\varepsilon = 2 * 10^{-1}$	4.114992	2.068582

5.2.2. Test case II. In the second test case, the real magnetic field data is given as a rectangle area with length=14040m, width=8720m, and the interval between each grids is 20m. The real magnetic field is defined by a two-dimensional grid of 702 by 436 as shown in Figure 13.

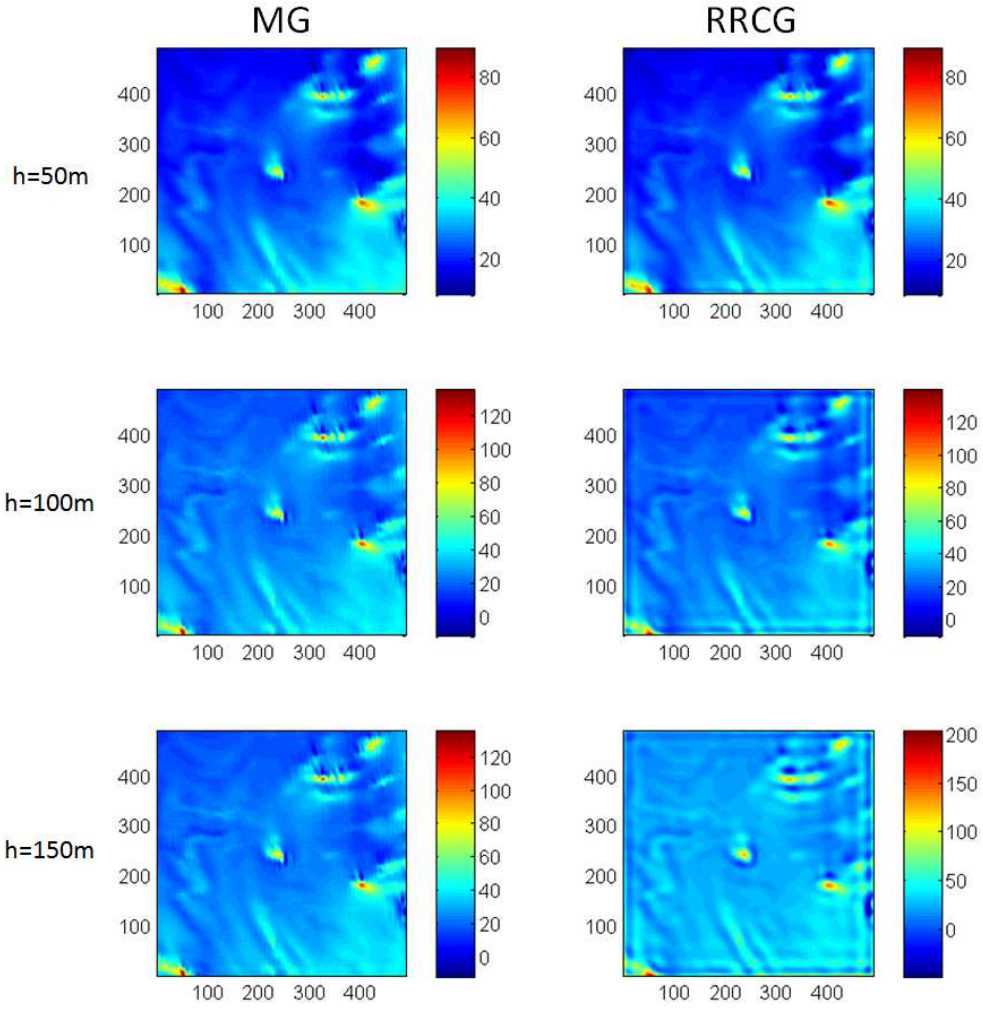

FIGURE 10. Inversion results for test case I with tolerance $3 * 10^{-1}$.

To evaluate the two numerical inversion schemes, Figure 14 presents the computed solutions using RRCG and MG methods at a fixed depth h=100m for tolerance $1 * 10^{-1}$, $5 * 10^{-2}$ and $1 * 10^{-2}$. In Figure 15, the inversion results at various depths h=50m, 100m and 150m are illustrated. The computing time required by the two methods are reported in Table 8.

From the results applied to test case II, we note that when the depth h is small, the inversion results produced by RRCG and MG methods are very similar. However, the discrepancy in terms of the maximum and minimum magnetization become noticeable as the depth increases and when the tolerance is decreasing. It is noted that both methods are capable of capturing similar underground geological features, but the RRCG produces larger artifacts near the boundary. The superior performance of the MG method over the RRCG is also clearly demonstrated by the significant saving in computing time as shown in Table 8.

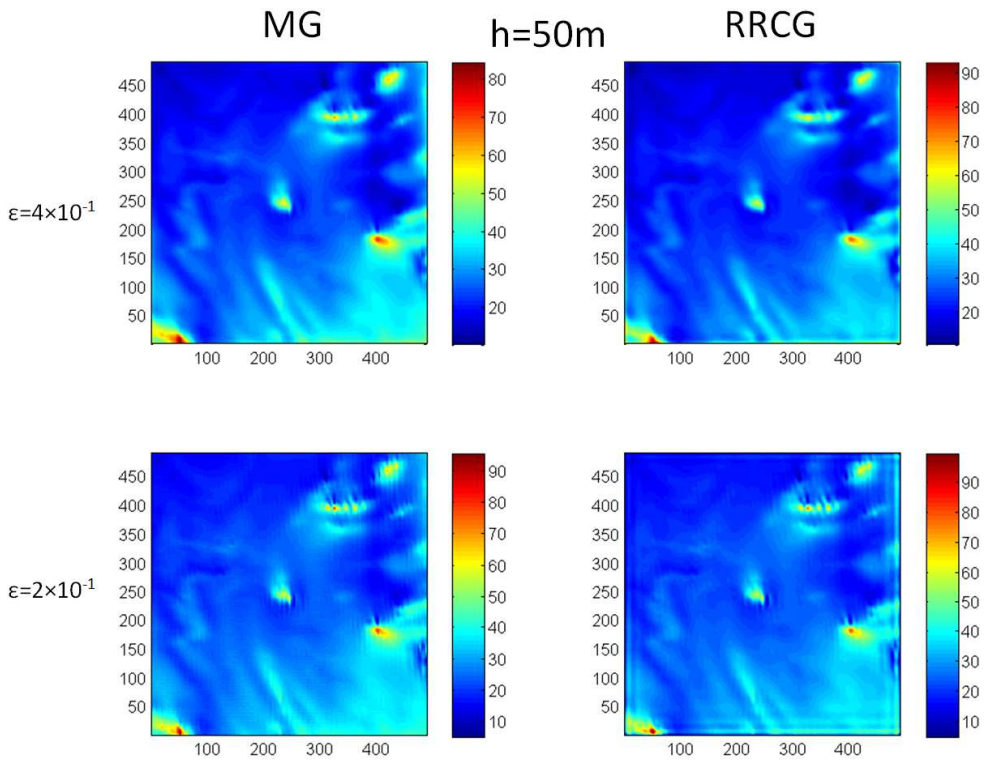

FIGURE 11. Inversion result for test case I at depth h=50m.

TABLE 8. The computing time for test case II.

Depth (m)	Tolerance	T_{RRCG} (s)	T_{MG} (s)
100	$\varepsilon = 1 * 10^{-1}$	2.626800	0.700371
100	$\varepsilon = 5 * 10^{-2}$	8.858662	2.744200
100	$\varepsilon = 1 * 10^{-2}$	144.395461	46.382697
50	$\varepsilon = 1 * 10^{-2}$	33.221171	15.612463
200	$\varepsilon = 1 * 10^{-2}$	352.861550	75.893122

6. Conclusion

In developing numerical inversion schemes for magnetization using uniform grid spacing, it is important to recognize that the inversion results can be computed by solving a symmetric Block-Toeplitz Toeplitz-Block (BTTB) system. The linear system is frequently large, dense and ill-conditioned. Direct implementation of the matrix coefficients will require considerable storage and leading to the requirement of large computing resources for the solution. By taking advantages of a symmetric BTTB property, the storage requirement can be reduced from $O(N^2)$ to $O(N)$ and the computational work for a typical iterative scheme decreases to $O(N \log N)$ instead of $O(N^2)$. Therefore, efficient numerical inversion schemes can be developed, and they are capable of dealing with a large scale inversion problem.

Several numerical inversion schemes have been investigated, and it has been demonstrated that the RRCG and MG methods are effective numerical tools for the inversion problems. Both methods have been tested to problems generated by

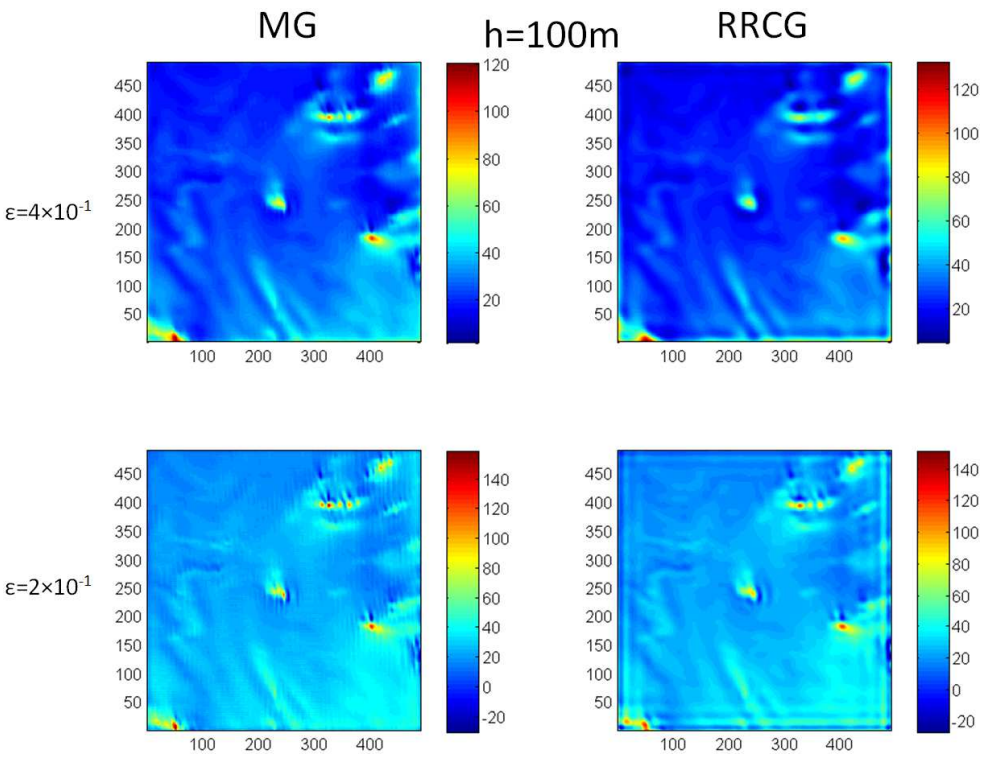

FIGURE 12. Inversion result for test case I at depth h=100m.

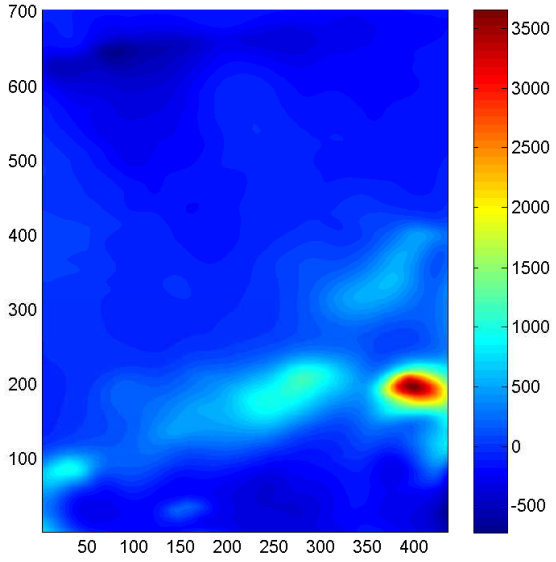

FIGURE 13. Test case II.

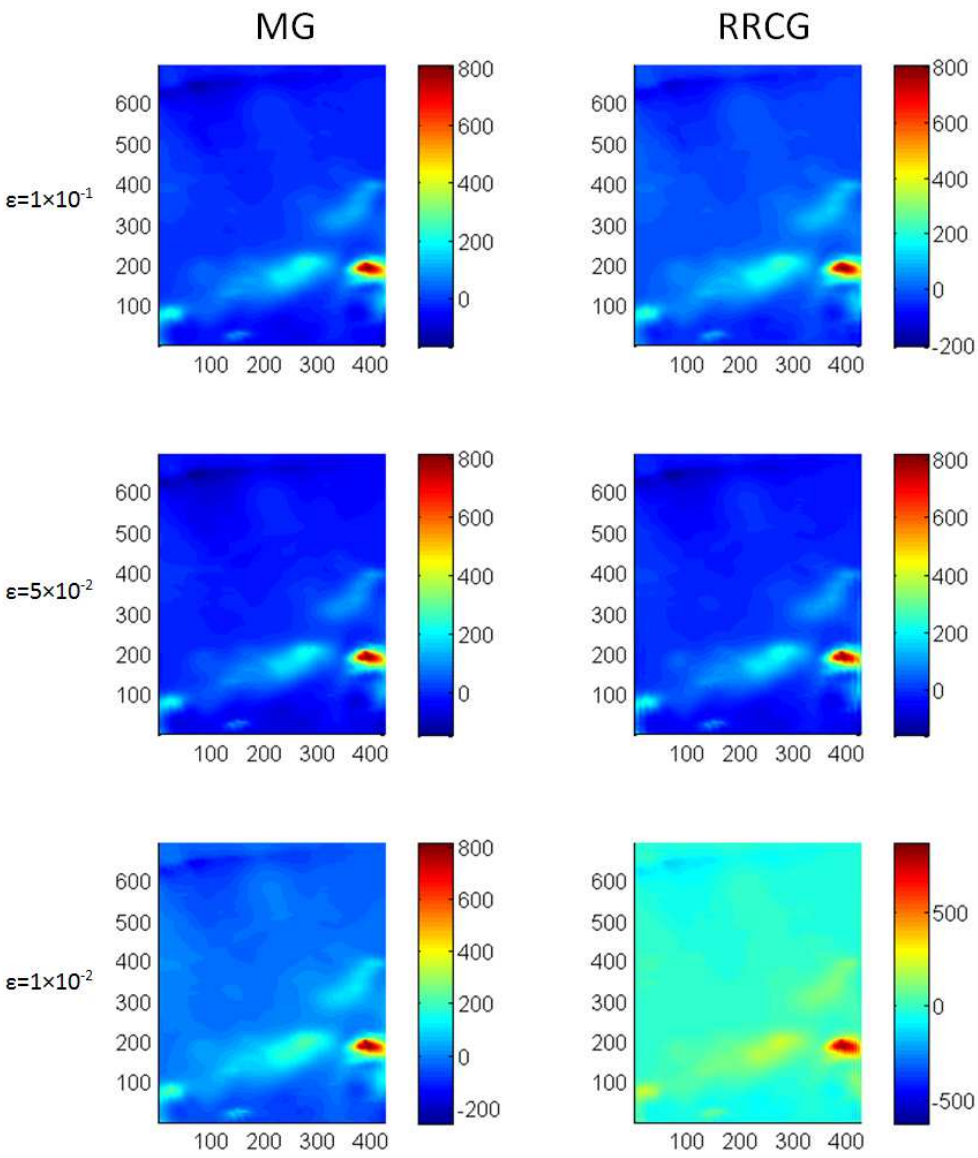

FIGURE 14. Inversion result for test case II at $h = 100$m.

synthetic data and real magnetic field data. Based on the computational simulation, we conclude that the MG technique has a superior performance compared to the RRCG method, in particular, the artifact near the boundary resulting from MG is much less than that produced by the RRCG. Moreover, significant saving in computing time is achieved by the MG for all cases tested in this paper. The MG method can be generalized to inversion problems with nonuniform grid spacing and to 3D problems.

References

[1] M. B. Allen and E. L. Isaacson, Numerical analysis for applied science, vol. 35, John wiley & sons, 2011.

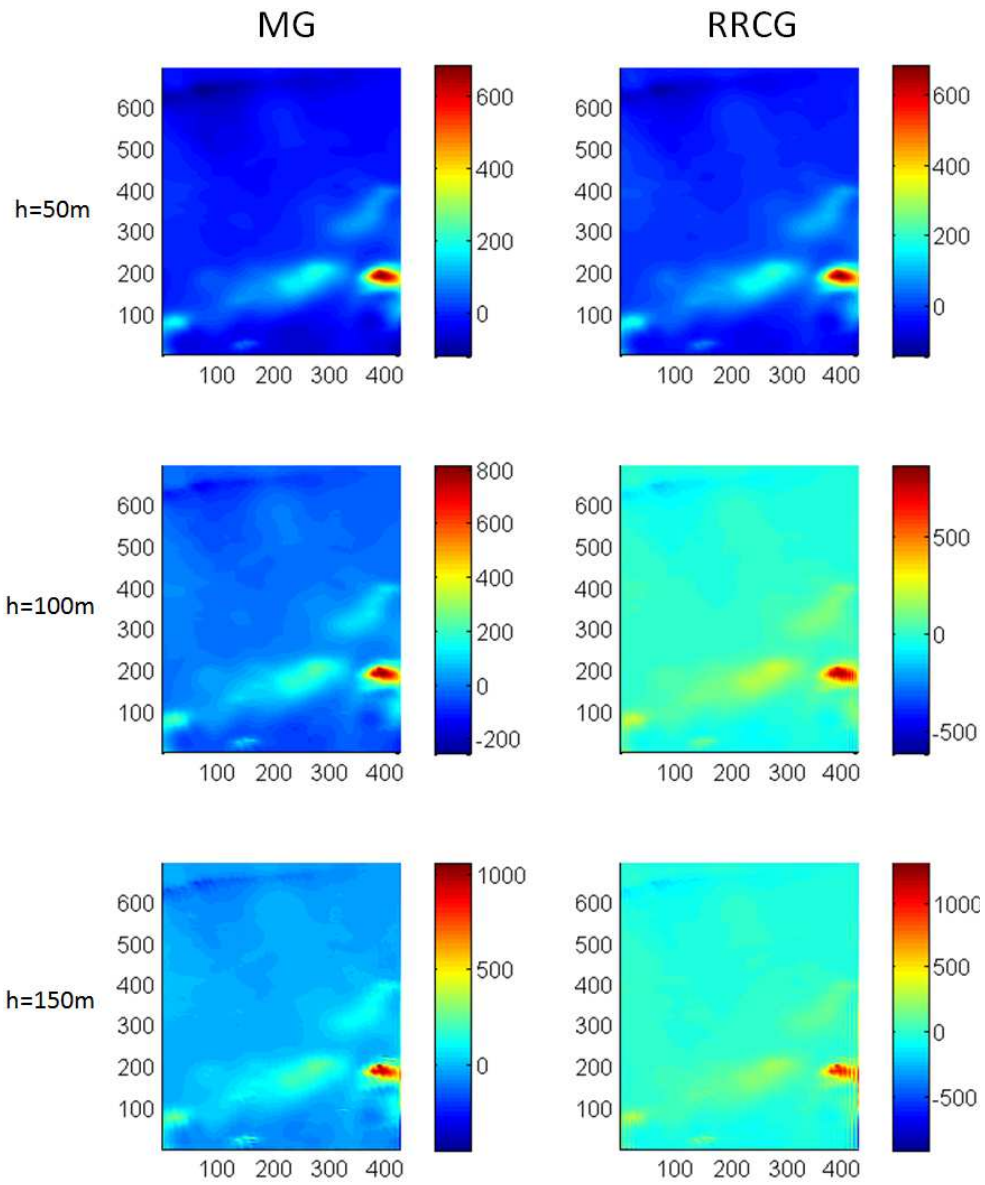

FIGURE 15. Inversion result for test case II with tolerance $= 1 * 10^{-2}$.

[2] H. R. Babu, A. Subrahmanyam, and D. A. Rao, A comparative study of the relation figures of magnetic anomalies due to two-dimensional dike and vertical step models, Geophysics, 47 (1982) 926–931.
[3] R. J. Blakely, Potential theory in gravity and magnetic applications, Cambridge University Press, 1996.
[4] I. C. Briggs, Machine contouring using minimum curvature, Geophysics, 39 (1974) 39–48.
[5] W. L. Briggs and S. F. McCormick, A multigrid tutorial, vol. 72, Siam, 2000.
[6] R. H. Chan, Circulant preconditioners for hermitian toeplitz systems, SIAM Journal on Matrix Analysis and Applications, 10 (1989) 542–550.
[7] R. H. Chan and X. Q. Jin, An introduction to iterative Toeplitz solvers, vol. 5, SIAM, 2007.
[8] R. H. Chan, J. G. Nagy, and R. J. Plemmons, Fft-based preconditioners for toeplitz-block least squares problems, SIAM journal on numerical analysis, 30 (1993) 1740–1768.

[9] R. H. Chan and M. K. Ng, Conjugate gradient methods for toeplitz systems, SIAM review, 38 (1996) 427–482.
[10] R. H. Chan and G. Strang, Toeplitz equations by conjugate gradients with circulant preconditioner, SIAM Journal on Scientific and Statistical Computing, 10 (1989) 104–119.
[11] G. Cooper, Gridding gravity data using an equivalent layer, Computers & Geosciences, 26 (2000) 227–233.
[12] L. Cordell, A scattered equivalent-source method for interpolation and gridding of potential-field data in three dimensions, Geophysics, 57 (1992) 629–636.
[13] K. Davis and Y. Li, Fast solution of geophysical inversion using adaptive mesh, space - filling curves and wavelet compression, Geophysical Journal International, 185 (2011) 157–166.
[14] P. J. Davis, Circulant matrices, New York, 1979 (1979).
[15] S. P. Gay Jr, Standard curves for interpretation of magnetic anomalies over long tabular bodies, Geophysics, 28 (1963) 161–200.
[16] P. C. Hansen, The L-curve and its use in the numerical treatment of inverse problems, IMM, Department of Mathematical Modelling, Technical Universityof Denmark, 1999.
[17] T. K. Ku and C. C. Kuo, Design and analysis of toeplitz preconditioners, Signal Processing, IEEE Transactions on, 40 (1992) 129–141.
[18] Y. Li and D. W. Oldenburg, 3-d inversion of magnetic data, Geophysics, 61 (1996) 394–408.
[19] C. A. Mendonca and J. B. Silva, Interpolation of potential-field data by equivalent layer and minimum curvature: A comparative analysis, Geophysics, 60 (1995) 399–407.
[20] M. Pilkington, 3-d magnetic imaging using conjugate gradients, Geophysics, 62 (1997) 1132–1142.
[21] D. A. Rao and H. R. Babu, Nomograms for rapid evaluation of magnetic anomalies over long tabular bodies, pure and applied geophysics, 119 (1981) 1037–1050.
[22] R. Rao, V. Vijayakumar, G. Virupakshi, and M. Rao, A note on the interpretation of magnetic anomalies of infinite thin sheets by using relation figures, Geophysical prospecting, 33 (1985) 746–752.
[23] M. Rauth and T. Strohmer, Smooth approximation of potential fields from noisy scattered data, Geophysics, 63 (1998) 85–94.
[24] G. Strang, A proposal for toeplitz matrix calculations, Studies in Applied Mathematics, 74 (1986) 171–176.
[25] H. W. Sun, X. Q. Jin, and Q. S. Chang, Convergence of the multigrid method of ill-conditioned block toeplitz systems, BIT Numerical Mathematics, 41 (2001) 179–190.
[26] J. Vanthienen, C. Mues, G. Wets, and K. Delaere, A tool-supported approach to inter-tabular verification, Expert systems with applications, 15 (1998) 277–285.
[27] M. Zhdanov, Geophysical inverse theory and regularization problems: Methods in geochemistry and geophysics, 2002.

Department of Mathematical and Statistical Sciences, University of Alberta, Alberta, T6G 2G1, Canada
E-mail: yile2@ualberta.ca, yauwong@ualberta.ca and deng2@ualberta.ca
URL: http://www.mathstats.ualberta.ca/

TerraNotes Ltd Geophysics, Canada
E-mail: shaleius@hotmail.com and terranotes@gmail.com
URL: http://www.terranotes.com/